A R C H I V E O F M E C H A N I C A L E N G I N E E R I N G

VOL. LXV 2018 Number 3

DOI: 10.24425/124488

Key words: bomb, flight dynamics, guided munition

MARIUSZ JACEWICZ[1], *ROBERT GŁĘBOCKI*[1], *ADRIAN SZKLARSKI*[1]

MINIATURE BOMB CONCEPT FOR UNMANNED AERIAL VEHICLES

This paper presents the design methodology of a small guided bomb for Unmanned Aerial Vehicles. This kind of next-generation munition has recently gained a lot of attention in the military market. The bomb is planned to be equipped with inertial measurement unit and infrared seeker. The nose shape and fin optimization procedure was described shortly. Aerodynamic characteristics were calculated by means of theoretical and engineering-level methods. The flight dynamics model of the bomb was obtained and implemented in Simulink software. The numerical simulations of uncontrolled and controlled trajectories were compared. The results indicate that the usage of such a guided small munition, like the designed bomb, might improve significantly the offensive capabilities of Unmanned Aerial Vehicles.

Nomenclature

b	bomb wing span
c_a	fin mean aerodynamic chord
c_k, c_p	fin tip chord and root chord, respectively
$C_L\ C_M,\ C_N$	rolling, pitching and yawing moment coefficients
C_{LP}	rolling moment coefficient derivative with roll rate
C_{MQ}	pitching moment coefficient derivative with pitch rate
C_{NR}	yawing moment coefficient derivative with yaw rate
$c_{xn},\ c_x$	nose and fin drag coefficients, respectively
$C_{x\,\min},\ C_{x\,\min_{od}}$	fin minimum and minimum empirical drag coefficients
$C_X,\ C_Y,\ C_Z$	axial, side and normal force coefficients
c_z	total fin lift coefficient

[1] *Institute of Aeronautics and Applied Mechanics, Warsaw University of Technology, Nowowiejska 24, 00-665 Warsaw, Poland. Emails: mjacewicz@meil.pw.edu.pl, rglebocki@meil.pw.edu.pl, aszklarski@meil.pw.edu.pl*

d	bomb fuselage maximum diameter
$e_0,\ e_1,\ e_2,\ e_3$	quaternion elements
$X_b,\ Y_b,\ Z_b$	axial, side and normal forces in body axes $O_b x_b y_b z_b$
F	nose shape function
$\mathbf{F}_a,\ \mathbf{M}_a$	aerodynamic forces and moments, respectively
$\mathbf{F}_b,\ \mathbf{M}_b$	total forces and moments in body frame $O_b x_b y_b z_b$
$\mathbf{F}_c,\ \mathbf{M}_c$	control forces and moments in body frame $O_b x_b y_b z_b$
$\mathbf{F}_g,\ \mathbf{M}_g$	gravity forces and moments in body frame $O_b x_b y_b z_b$
$I_x,\ I_y,\ I_z$	moments of inertia
$I_{xy},\ I_{xz},\ I_{yz}$	products of inertia
l_n	bomb nose section length
$L_b,\ M_b,\ N_b$	rolling, pitching and yawing moments in body axes $O_b x_b y_b z_b$
m	bomb total mass
Ma	Mach number
q	dynamic pressure
$P,\ Q,\ R$	angular rates
Re	Reynolds number
S	reference area
$S_x,\ S_y,\ S_z$	static moments
t	airfoil thickness
$U,\ V,\ W$	linear velocities in body frame $O_b x_b y_b z_b$
V_0	total flight velocity
$X_b,\ Y_b,\ Z_b$	axial, side and normal forces in body frame $O_b x_b y_b z_b$
y	value of the nose shape function
$\alpha,\ \beta$	angles of attack and sideslip, respectively
$\alpha_{\min},\ \alpha_{\max}$	minimum and maximum bomb angles of attack
$\delta,\ \delta_1,\ \delta_2,\ \delta_3$	Glauert's correction coefficients
$\delta_A,\ \delta_B,\ \delta_C,\ \delta_D$	control surfaces deflection angles
$\Phi,\ \Theta,\ \Psi$	Euler angles (roll, pitch and yaw)
ρ	air density
$\tau,\ \tau_1,\ \tau_2,\ \tau_3$	Glauert's correction coefficients
$\lambda,\ \Lambda$	fin taper ratio and aspect ratio

1. Introduction

The presented work was inspired by current development tendencies of the small bomb intended for tactical Unmanned Aerial Vehicles (UAV). In the last years, one can observe that the usage of the small UAVs on the modern battlefield

becomes more and more important. One of the most significant tasks for this type of flying objects is to ensure the reconnaissance for the ground troops. The usage of UAVs is a cost-effective way to destroy the stationary small objects like trucks, bunkers or boats. The significant problem is the lack of existing small guided bombs. An unguided bomb has inadequate accuracy of hitting moving targets. With the usage of a light bombs, a tactical UAV can preserve its flight endurance capabilities and can realize new offensive tasks, which can made this type of munition very attractive for potential users.

2. State of the art

There exist only a few bombs intended specially for UAVs. One of the examples of such a munition is the Free-Fall Lightweight Multi-role Missile (FFLMM) developed by Thales (Fig. 1a). The weight of the bomb is 6 kg, length 700 mm and the warhead weight 2 kg [1]. The stationary and moving targets can be destroyed with a minimum risk of causing unwanted damage, e.g., civil casualties. The bomb uses INS and GPS navigation systems. A semi-active laser guidance is also used during the last stage of flight to hit the target.

The second example of a small guided bomb is Bozok (Fig. 1b), which is designed by Roketsan [2]. This bomb belongs to the Miniature Laser Guided Munition type. The range is 8 km and it depends of the launch altitude. Bomb mass is 16 kg, length 800 mm and wingspan 120 mm. When the bomb is dropped at an altitude of 6 km with initial velocity 50 m/s, then the range is 9 km.

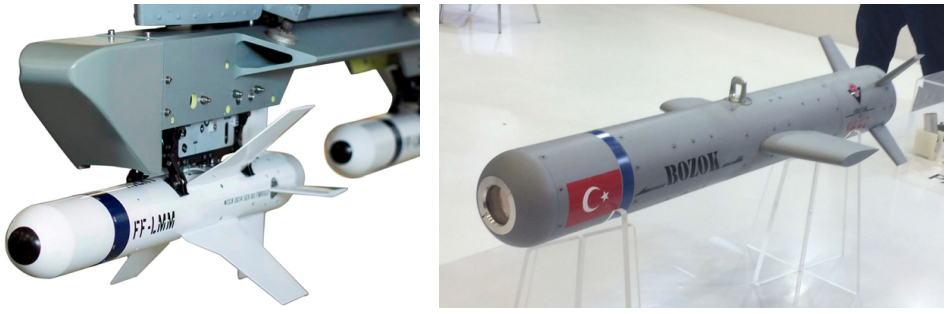

(a) (b)

Fig. 1. Two examples of the small guided bombs for UAV: (a) Free-Fall Lightweight Multi-role Missile (from Thales) [1]; (b) Bozok bomb [2]

The usage of small UAVs as a munition carriers can be a very doubtful from ethics standpoint and in the law enforcement contexts. Some experts claim that usage of this type of munition should be regulated by some war conventions because a misuse may occur there during warfare.

3. Bomb design requirements and methodology

The following section presents the concept of the bomb. The most important requirements for the bomb are assumed as follows [3, 4]:

- maximum mass lower than 10 kg,
- range at least 20 km when dropped from 7000 m,
- controlled trajectory flight capabilities,
- integrated INS and infrared guidance [5],
- UAV integration capabilities,
- minimal unwanted damage risk (influence warhead type).

It was decided that the GPS will not be used in the guidance loop because of the potential risk of jamming during warfare. Pure aerodynamic control will be used to meet the controlled trajectory requirements [6]. Other control methods, like reaction control system presented in [7] or thrust vectoring, are not applicable due to rigorous mass constraint.

The basic configuration of the bomb is presented in Fig. 2 and it consists of: the cylindrical fuselage, two fins sets and the seeker mounted at the nose of the bomb. Each fin set consists of four trapezoidal fins. Both fin sets are rotated mutually by 45 deg, which improves the bomb aerodynamic characteristics [8]. The forward fin set is in "+" configuration while the rear fins are placed in "x" orientation and are used as movable aerodynamic control surfaces. Maximum allowable deflections are 7 deg. Mass of the bomb is designed to be equal 8 kg, which is much less than initial requirements.

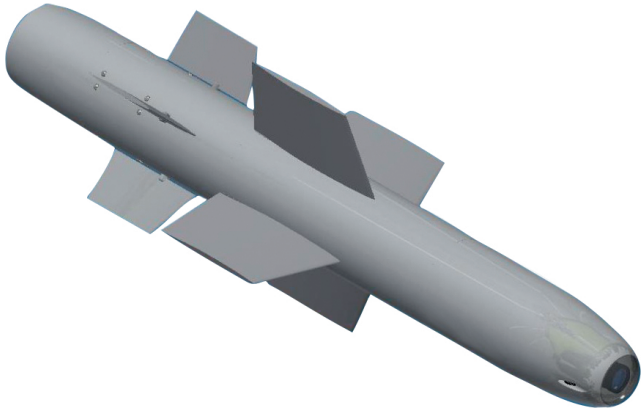

Fig. 2. The 3D CAD drawing of the designed bomb

The usage of composite parts in the construction will be maximized to achieve the minimum mass. It is planned that the prototype of the bomb will be equipped with a parachute to save the bomb after the flight tests.

4. Detailed bomb design

In this section, we present some details from overall aerodynamic design stage. All the components were defined separately. Computational Fluid Dynamics, analytical calculations, engineering semi-empirical codes, wind tunnel or flight tests might be used to design and improve the bomb aerodynamic characteristics [9]. During bomb preliminary design stage, analytical and engineering-level, semi-empirical methods were used to obtain aerodynamic coefficients.

4.1. Nose cone definition

The main goal during the nose cone definition process was to obtain the minimum pressure drag. This task is not so easy to fulfill, because of the seeker at nose bomb location requirement [10]. In the presented case, the shape of the nose part of the bomb must be obtained. For the subsonic speeds (0–0.8 Ma) the Newton hypothesis was used to determine the total drag P_x of the nose section [3]. The elementary normal force is equal to:

$$dR = \rho\, dQ\, v(1 - \cos\theta), \tag{1}$$

where: dQ – elementary volume flow rate, v – undisturbed flow velocity, θ – surface pitch angle due to undisturbed flow.

The total pressure drag can be calculated as [3]:

$$P_X = 2\pi q \int_0^{l_n} y \frac{\dot{y}^4}{1 + \dot{y}^2}\, \mathrm{d}\, x, \tag{2}$$

where: y – value of the function which describes the nose shape, x – length parameter.

The nose function F might be approximated as [3]:

$$F\,(y, \dot{y}) = y\dot{y}^4. \tag{3}$$

The task was to minimize the functional [3]:

$$I[y] = \int_0^{l_n} y\dot{y}^4\, \mathrm{d}\, x. \tag{4}$$

Using the above equations, one can calculate the nose drag coefficient as [3], [6]:

$$c_x = \frac{8}{d^2} \int_0^{l_n} y\dot{y}^4\, \mathrm{d}\, x. \tag{5}$$

The results of the used method and the nose shape are presented in Fig. 3. On the horizontal and vertical axes, the coordinates were undimensionalized by nose length l_n and bomb fuselage radius $d/2$.

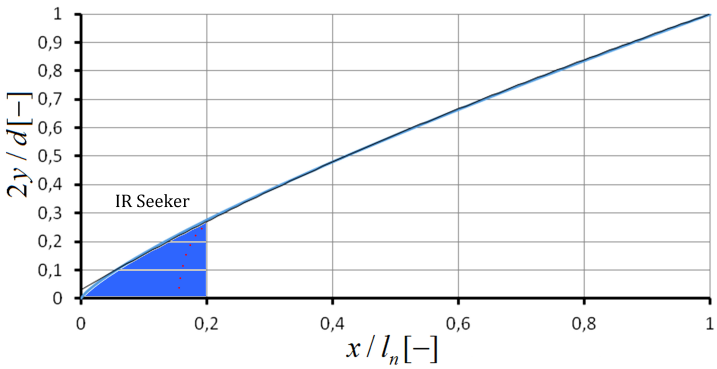

Fig. 3. The nose shape function values

The vales of the nose function F were corrected and the front part of the nose was rounded to ensure the seeker location (blue area in Fig. 3).

4.2. Fuselage geometric shape definition

The fuselage of the bomb was assumed to be a cylinder. The main elements which must be placed inside the fuselage are: the seeker, the warhead, the set of servomechanisms, the battery unit and the navigation unit (Fig. 4). The external diameter of the fuselage was constrained by the UAV type and the warhead mass. A boat tail was added to optimize the base pressure drag [6].

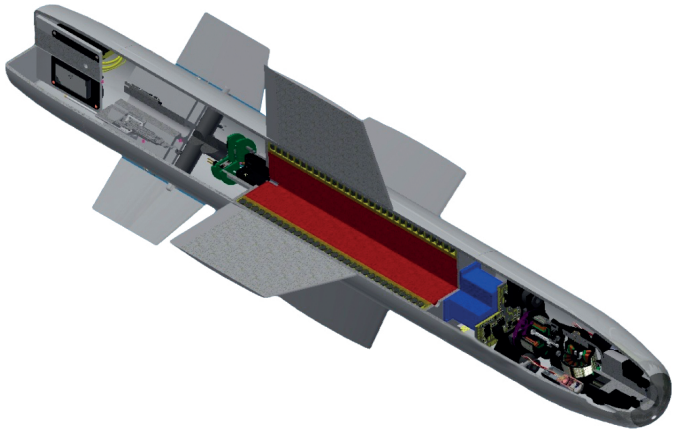

Fig. 4. The bomb cutaway drawing with main elements placed inside the fuselag

4.3. Fin definition

The main goal of this stage was to obtain satisfactory stability margin. The overall calculation process was performed in a two-step method. First the shape of the fins was designed, then the bomb stabilization corrections were included.

4.3.1. Step 1: fin shape project

The next step in the overall process was to calculate the fin polar curve. The method presented in [6] was used at this stage and the input data were as follows:

- fin span $b = 0.2$ m,
- root chord $c_p = 0.12$ m,
- tip chord $c_k = 0.08$ m,
- mean aerodynamic chord $c_a = 0.1$ m,
- airfoil thickness $t = 0.003$ m.

The lift coefficient was assumed to be linear in the range between the minimum $\alpha_{\min}$ and the maximum $\alpha_{\max}$ angles of attack. The average value of the lift coefficient derivative with respect to angle of attack is:

$$\frac{dc_z}{d\alpha} = 5.73\,\frac{1}{\text{rad}}. \tag{6}$$

The taper ratio to the above derivative ratio is equal to:

$$\frac{\Lambda}{\dfrac{dc_z}{d\alpha}} = 0.35. \tag{7}$$

The Glauert's coefficients [6] were calculated as $\tau_1' = 0.17$, $\delta_1' = 0.048$, $\tau_2' = 0.278$, $\delta_2' = 0.12$, $\tau_3' = 0.58$, $\delta_3' = 0.05$. So, the total Glauert's coefficients are: $\tau = 0.95$ and $\delta = 0.125$. The polar curve was approximated as:

$$c_x = c_{x\infty} + c_z^2\frac{(1+\delta)}{\pi\Lambda} = c_{x\infty} + 0.179c_z^2\,. \tag{8}$$

The angle of attack correction was introduced as follows:

$$\alpha^0 = \alpha_\infty^0 + c_z\frac{(1+\tau)}{\pi\Lambda} = \alpha_\infty^0 + 0.31c_z\,. \tag{9}$$

4.3.2. Step 2: bomb stabilization

The bomb stabilization problem was treated and solved as an iterative process [6]. Because of the subsonic bomb flight velocity, the air compressibility was neglected. So, the fin lift coefficient depended on the angle of attack α, the fin taper ratio λ and the fuselage cross section:

$$c_{yub} = f(\alpha, \lambda, S). \tag{10}$$

When the $c_{yub} = f(\alpha, \lambda, S)$ coefficient was known, the location of fins with respect to the bomb center of mass was calculated. The stability margin was obtained to be 3.1% of the total bomb length. The bomb cannot have too big stability margin because of the maneuverability capabilities [11].

5. Flight simulation model

In this section, the bomb flight dynamics model is described. It is very important to confirm the bomb predicted characteristics by means of numerical methods before the flight tests. Aerodynamic characteristics were obtained with the use of the presented earlier calculations.

5.1. Physical model

It is assumed that the simulated bomb is a rigid body with six deegres of freedom. The mass of the bomb is assumed to be 8 kg, diameter 80 mm, the length 665 mm. The center of mass is located 317 mm from the nose. The object is controlled by means of four fins located behind the center of mass (Fig. 5). The bomb has two geometric, mass and aerodynamic symmetry planes. Due to the relatively short range, the flat and non-rotating Earth approximation was used. The wind influence on bomb trajectory was neglected.

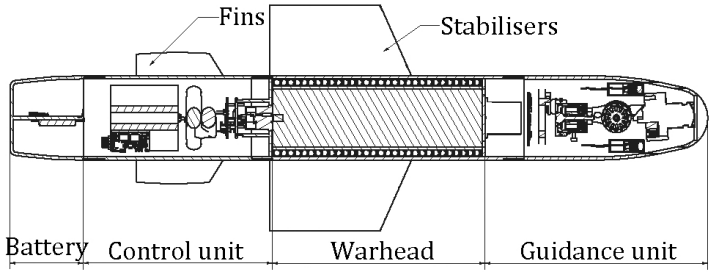

Fig. 5. Bomb assembly

5.2. Mathematical model

In this section, the mathematical model is described. The navigation coordinate system $O_n x_n y_n z_n$, the body-fixed coordinate system $O_b x_b y_b z_b$ and the gravity system $O_g x_g y_g z_g$ (Fig. 6) were used to describe the bomb motion.

The origin O_n of the $O_n x_n y_n z_n$ coordinate system is an arbitrary point on the Earth surface. The $O_n x_n z_n$ plane is horizontal, tangent to the earth surface, the $O_n x_n$ axis points to the North, and $O_n y_n$ axis to the East.

The body-fixed $O_b x_b y_b z_b$ frame is rigidly attached to the bomb. The center O_b lies in the center of mass of the bomb at an arbitrary point in the bomb axis

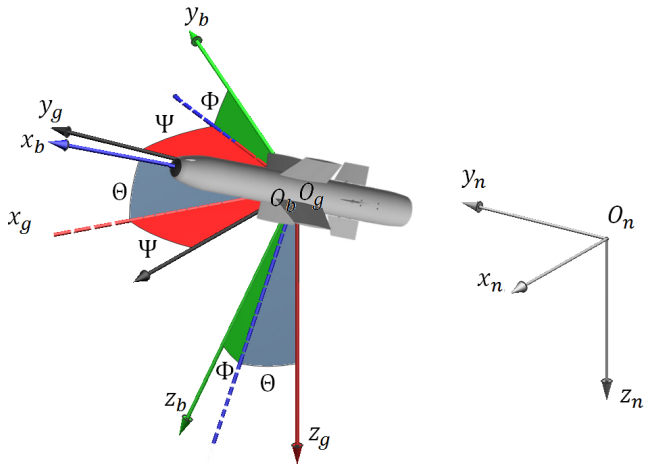

Fig. 6. Navigation $O_n x_n y_n z_n$, gravity $O_g x_g y_g z_g$ and body $O_b x_b y_b z_b$ fixed coordinated systems

of symmetry. The $O_b x_b$ axis lies in the axis of bomb symmetry and is directed forward. The $O_b y_b$ axis is perpendicular to the axis of bomb symmetry and points right, the $O_b z_b$ axis points down.

The origin O_g of the gravity coordinate system $O_g x_g y_g z_g$ coincides with O_b and the axis are parallel to the axis of $O_n x_n y_n z_n$ coordinate system.

The Euler angles: Φ – roll, Θ – pitch and Ψ – yaw were used to describe the mutual orientation of the $O_b x_b y_b z_b$ with respect to $O_g x_g y_g z_g$.

Equation of motion of the bomb in the $O_b x_b y_b z_b$ coordinate system is as follows [7, 12]:

$$\mathbf{Ax} + \mathbf{\Omega Ax} = [\mathbf{F}_b \;\; \mathbf{M}_b]^{\mathrm{T}}, \tag{11}$$

where:

$$\mathbf{x} = [U \;\; V \;\; W \;\; P \;\; Q \;\; R]^{\mathrm{T}}. \tag{12}$$

The inertia matrix is defined as [12]:

$$\mathbf{A} = \begin{bmatrix} m & 0 & 0 & 0 & 0 & 0 \\ 0 & m & 0 & 0 & 0 & 0 \\ 0 & 0 & m & 0 & 0 & 0 \\ 0 & 0 & 0 & I_x & 0 & 0 \\ 0 & 0 & 0 & 0 & I_y & 0 \\ 0 & 0 & 0 & 0 & 0 & I_z \end{bmatrix}, \tag{13}$$

It was assumed that the bomb is an axisymmetric body, so the products of inertia I_{xy}, I_{xz}, I_{yz} are zero.

The matrix of velocities and angular rates is as below [12]:

$$\mathbf{\Omega} = \begin{bmatrix} 0 & -R & Q & 0 & 0 & 0 \\ R & 0 & -P & 0 & 0 & 0 \\ -Q & P & 0 & 0 & 0 & 0 \\ 0 & -W & V & 0 & -R & Q \\ W & 0 & -U & R & 0 & -P \\ -V & U & 0 & -Q & P & 0 \end{bmatrix}. \tag{14}$$

The relation between velocities in $O_b x_b y_b z_b$ and $O_n x_n y_n z_n$ can be determined as [7, 12]:

$$\begin{bmatrix} \dot{x}_n \\ \dot{y}_n \\ \dot{z}_n \end{bmatrix} = \\ = \begin{bmatrix} \cos\Theta\cos\Psi & \cos\Theta\sin\Psi & \sin\Theta \\ \sin\Phi\sin\Theta\cos\Psi - \cos\Phi\sin\Psi & \sin\Phi\sin\Theta\sin\Psi + \cos\Phi\cos\Psi & \sin\Phi\cos\Theta \\ \cos\Phi\sin\Theta\cos\Psi + \sin\Phi\sin\Psi & \cos\Phi\sin\Theta\sin\Psi - \sin\Phi\cos\Psi & \cos\Phi\cos\Theta \end{bmatrix} \begin{bmatrix} U \\ V \\ W \end{bmatrix}. \tag{15}$$

Given the body angular rates P, Q, R, the bomb attitude can be obtained through a set of kinematic constraints [7, 12]:

$$\begin{bmatrix} \dot{e}_0 \\ \dot{e}_1 \\ \dot{e}_2 \\ \dot{e}_3 \end{bmatrix} = -\frac{1}{2} \begin{bmatrix} 0 & P & Q & R \\ -P & 0 & -R & Q \\ -Q & R & 0 & -P \\ -R & -Q & P & 0 \end{bmatrix} \begin{bmatrix} e_0 \\ e_1 \\ e_2 \\ e_3 \end{bmatrix} - kE \begin{bmatrix} e_0 \\ e_1 \\ e_2 \\ e_3 \end{bmatrix}. \tag{16}$$

The gain k drives the norm of the quaternion state vector to one. Next, the roll, pitch and yaw angles are calculated as below:

$$\Phi = \arctan\left[\frac{2(e_0 e_1 + e_2 e_3)}{e_0^2 - e_1^2 - e_2^2 + e_3^2}\right], \tag{17}$$

$$\Theta = \arcsin\left[2(e_0 e_2 - e_1 e_3)\right], \tag{18}$$

$$\Psi = \arctan\left[\frac{2(e_0 e_3 + e_1 e_2)}{e_0^2 + e_1^2 - e_2^2 - e_3^2}\right]. \tag{19}$$

Equations (11), (15) and (16) make a set of 12 differential equations that describe the motion of the bomb in three-dimensional space. Matrix notation was used due for the numerical purposes.

The total forces and moments acting on the rocket were calculated as a sum of the gravity, aerodynamic and control loads within the $O_b x_b y_b z_b$ coordinate frame [12]:

$$\mathbf{F}_b = \mathbf{F}_g + \mathbf{F}_a + \mathbf{F}_c\,, \tag{20}$$

$$\mathbf{M}_b = \mathbf{M}_g + \mathbf{M}_a + \mathbf{M}_c\,, \tag{21}$$

The forces and moments in the body frame are presented in the Fig. 7.

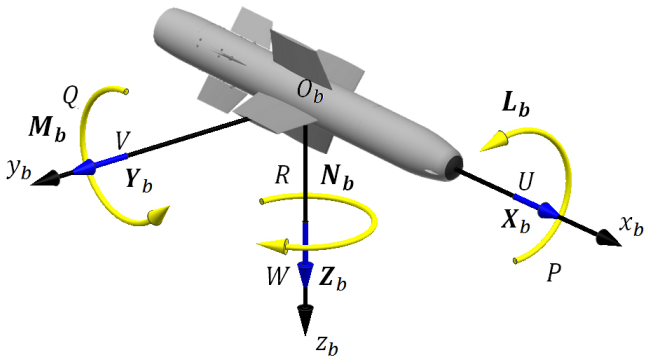

Fig. 7. Linear velocities, angular rates and loads in the body frame

The gravity forces $\mathbf{F}_g$ can be calculated as [7]:

$$\mathbf{F}_g = mg \begin{bmatrix} -\sin\Theta \\ \cos\Theta \sin\Phi \\ \cos\Theta \cos\Phi \end{bmatrix}. \tag{22}$$

It is assumed that the origin O_b of the body-fixed coordinate system is located in the rocket center of mass, so the moments from gravity forces are equal zero:

$$\mathbf{M}_g = \begin{bmatrix} 0 \\ 0 \\ 0 \end{bmatrix}. \tag{23}$$

Additionally, aerodynamic coordinate frame $O_a x_a y_a z_a$ was introduced to describe the aerodynamic loads (Fig. 8).

Angles of attack α and sideslip β were calculated as:

$$\alpha = \arctan \frac{W}{V_0}\,, \tag{24}$$

$$\beta = \arcsin \frac{V}{V_0}\,. \tag{25}$$

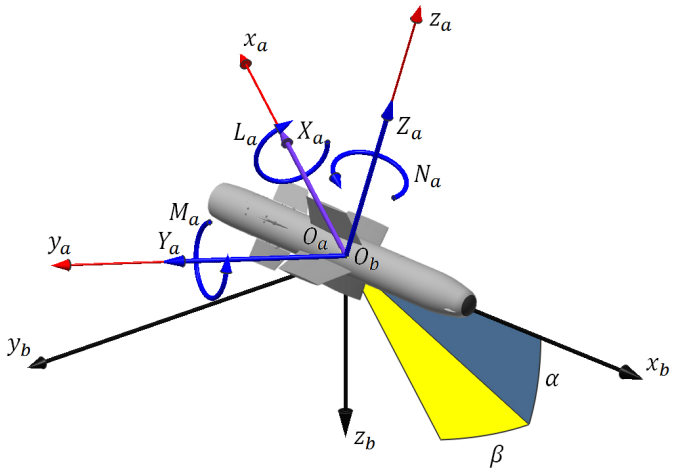

Fig. 8. Body and aerodynamic frames

The total flight velocity V_0 is defined as follows:

$$V_0 = \sqrt{U^2 + V^2 + W^2}\,. \tag{26}$$

The aerodynamic forces $\mathbf{F}_a$ in plain configuration in the $O_b x_b y_b z_b$ coordinate system are expressed in the following manner:

$$\mathbf{F}_a = \frac{1}{2}\rho V_0^2 S \begin{bmatrix} -C_X(\alpha,\beta,\mathrm{Ma}) \\ C_Y(\alpha,\beta,\mathrm{Ma}) \\ -C_Z(\alpha,\beta,\mathrm{Ma}) \end{bmatrix}, \tag{27}$$

and the similar moments:

$$\mathbf{M}_a = \frac{1}{2}\rho V_0^2 S d \begin{bmatrix} -C_L(\alpha,\beta,\mathrm{Ma})\delta - \dfrac{P}{2V_0} C_{LP}(\alpha,\beta,\mathrm{Ma}) \\ C_M(\alpha,\beta,\mathrm{Ma}) + \dfrac{Q}{2V_0} C_{MQ}(\alpha,\beta,\mathrm{Ma}) \\ -C_N(\alpha,\beta,\mathrm{Ma}) - \dfrac{P}{2V_0} C_{NP}(\alpha,\beta,\mathrm{Ma}) - \dfrac{R}{2V_0} C_{NR}(\alpha,\beta,\mathrm{Ma}) \end{bmatrix}, \tag{28}$$

The aerodynamic forces due to fins deflections $\mathbf{F}_c$ were calculated as:

$$\mathbf{F}_c = \begin{bmatrix} X_c \\ Y_c \\ Z_c \end{bmatrix} = \frac{1}{2}\rho V_0^2 S \begin{bmatrix} X_{\delta_A}\delta_A + X_{\delta_B}\delta_B + X_{\delta_C}\delta_C + X_{\delta_D}\delta_D \\ Y_{\delta_A}\delta_A + Y_{\delta_B}\delta_B + Y_{\delta_C}\delta_C + Y_{\delta_D}\delta_D \\ Z_{\delta_A}\delta_A + Z_{\delta_B}\delta_B + Z_{\delta_C}\delta_C + Z_{\delta_D}\delta_D \end{bmatrix}. \tag{29}$$

In a similar manner, control moments $\mathbf{M}_c$ were obtained as below:

$$\mathbf{M}_c = \begin{bmatrix} L_c \\ M_c \\ N_c \end{bmatrix} = \frac{1}{2}\rho V_0^2 S d \begin{bmatrix} L_{\delta_A}\delta_A + L_{\delta_B}\delta_B + L_{\delta_C}\delta_C + L_{\delta_D}\delta_D \\ M_{\delta_A}\delta_A + M_{\delta_B}\delta_B + M_{\delta_C}\delta_C + M_{\delta_D}\delta_D \\ N_{\delta_A}\delta_A + N_{\delta_B}\delta_B + N_{\delta_C}\delta_C + N_{\delta_D}\delta_D \end{bmatrix}, \tag{30}$$

where δ_A, δ_B, δ_C, δ_D are presented in Fig. 9.

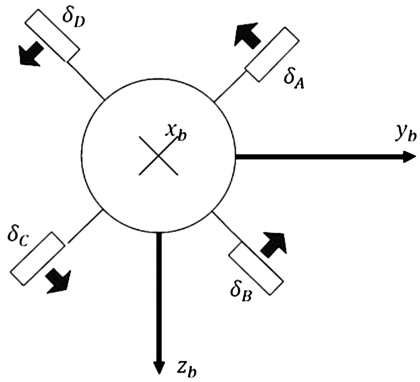

Fig. 9. Body and aerodynamic frames

The range of fins deflections can be described by the set of constraints:

$$\delta_{i_{\min}} \leqslant \delta_i \leqslant \delta_{i_{\max}}, \tag{31}$$

where $i = \{A, B, C, D\}$, $\delta_{i_{\min}}$ and $\delta_{i_{\max}}$ are minimum and maximum allowed deflection angles, respectively. The dynamics of the control surfaces deflection was modeled as a first-order transfer function with lag time:

$$\frac{\delta_i}{\delta_{i_c}} = \frac{1}{Ts+1} e^{-s\tau_d}, \tag{32}$$

where: T – time constants (was assumed be equal 0.12 s), δ_i – actual deflection angle, δ_{i_c} – commanded fin deflection angle, τ_d – fin deflection delay time (equal to 0.003 s).

The aerodynamic characteristics were assumed to be dependent on flight Mach number Ma, angles of attack α and sideslip β. Numerical values were obtained by handout methods and also compared with the results from the Fluent CFD software. The aerodynamic coefficients were calculated for various Mach numbers in range from 0.05 to 1.5. The transonic speed region was also modeled due to the possibility of interpolation errors. The linear interpolation was used between node values. Below, the drag force (Fig. 10a) and lift force (Fig. 10b) coefficients are presented. It is planned that the bomb will be roll-stabilized.

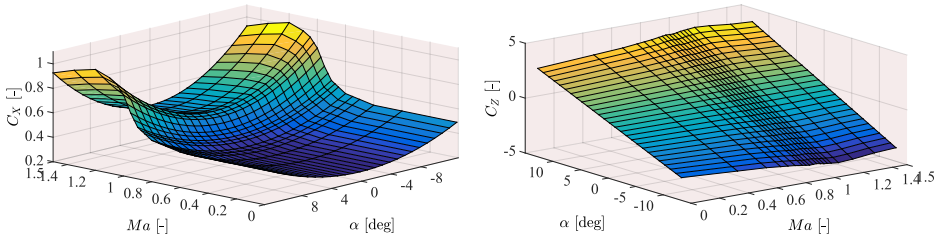

(a) (b)

Fig. 10. Aerodynamic forces coefficients as a function of angle of attack and Mach number: (a) bomb drag coefficient, (b) lift coefficient

6. Numerical experiments

In this section, there are presented the results of the numerical simulations. The previously described mathematical model was implemented in the Matlab software. The main goals of the experiments were to determine the stability characteristics, the range as a function of height and the fin set control effectiveness. First, the unguided flight was considered, next a number of control flight cases were performed. Both the longitudinal and lateral motions of the bomb were simulated. In Table 1, the initial conditions for simulations are presented. Only some chosen cases were shown. The initial pitch angle was assumed to be zero for all test cases.

Table 1.

Initial values of UAV flight parameters for bombing numerical simulation

No.	Drop altitude h [m]	Drop velocity V_{0in} [m/s]
1	1000	35
2	400	35
3	180	35
4	100	35
5	100	20

The initial velocities have quite a low values because of the UAV capabilities. In the plots of Figs. 11–13, there are presented the x_n distance, z_n coordinate (with minus) and pitch angle Θ as a function of time.

When the bomb was dropped from 1000 m, the range was about 495 m. It was a satisfactory result. The fifth case was different from the previous ones because of lower drop velocity.

The curves had a proper shape, which confirmed that the bomb had a sufficient stability margin. The altitude of UAV at the beginning of bomb flight was only 1000 m. The differences between two latter simulations were very small in the last plot, but are easy observable in the previous one.

In the course of flight time, the pitch angle decreases and is damped simultaneously, which proves that the bomb is statically stable. There are only small

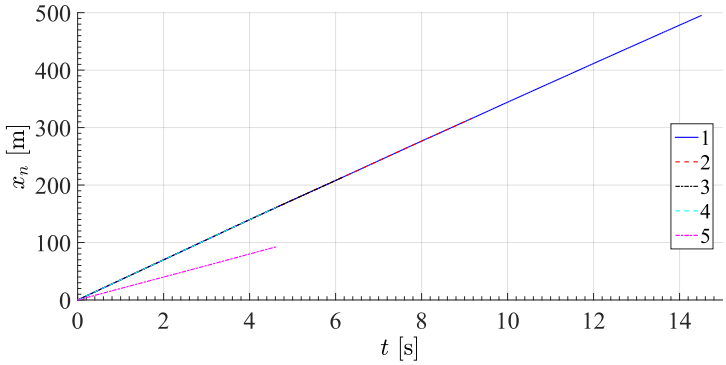

Fig. 11. Bomb range comparison for test cases

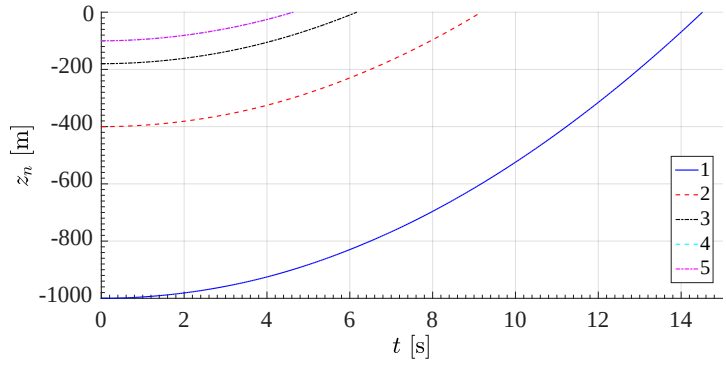

Fig. 12. Bomb height as a function of bomb drop altitude (in navigation coordinate system)

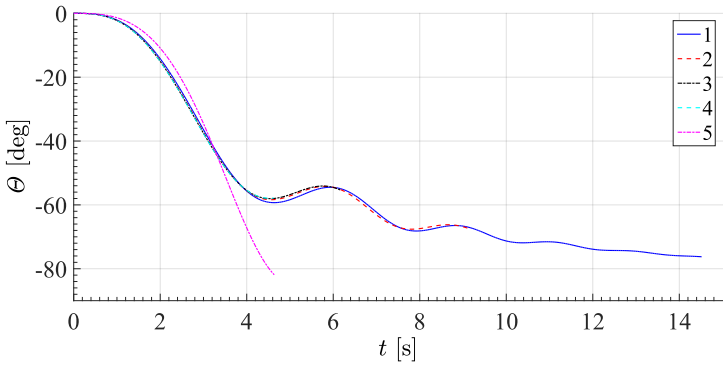

Fig. 13. Bomb pitch angle changes for unguided flight

differences between the cases from 1 to 4. In the case 5, the pitch angle decreases faster than in the previous ones because of low initial drop velocity. It is assumed that interference effects between UAV and a bomb are neglected but they will be included in the future. The Euler angles were used to describe the bomb motion.

This may lead to solution singularities when the pitch angle is 90 deg. Next, a set of the controlled flight simulations were performed to obtain the bomb maneuvering capabilities. The first case was an uncontrolled trajectory similar as in the previous simulations. The control fins were in "x" configuration, so it was necessary to combine all the deflection angles to modify the flight trajectory effectively. The step input was applied at the fifth second of the simulation. In the second case simulation, the fins δ_C and δ_D were deflected symmetrically at positive angles while the fins δ_A and δ_B had negative deflections. In the third simulation, the fins were deflected in opposite sides. Exactly in the same manner, the fourth and fifth ones for lateral motion were performed. The test cases are presented in Table 2.

Table 2.

Bomb fin deflection angles which were used in controlled flight simulations

No.	1	2	3	4	5
δ_{Ac} [deg]	0	–3	3	3	–3
δ_{Bc} [deg]	0	–3	3	–3	3
δ_{Cc} [deg]	0	3	–3	–3	3
δ_{Dc} [deg]	0	3	–3	3	–3

Below in Fig. 14, the total flight velocity V_0 is shown. In the plots of Figs 15–17, the x_n distance, the y_n distance, minus z_n coordinate are presented. Finally, the pitch Θ and yaw Ψ angles are depicted in Figs 18–19.

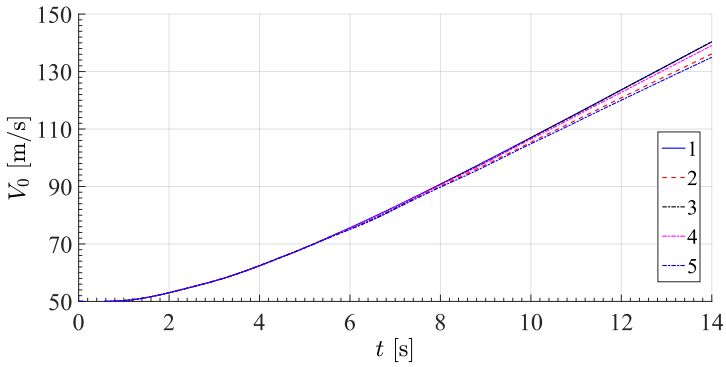

Fig. 14. Total flight velocity

The final flight velocity had the highest value for uncontrolled flight and for the third case when the bomb trajectory was curved down. The high velocity in the first case can be observed because of the low drag (no fin deflections). The maximum differences between final velocities at the impact at the ground moment are below 7 m/s.

The difference measured along y_n axis between uncontrolled and controlled flight cases is about 50 m. It is worth nothing that the fin deflection angles were only 3 deg, when the maximum allowable deflection was 7 deg.

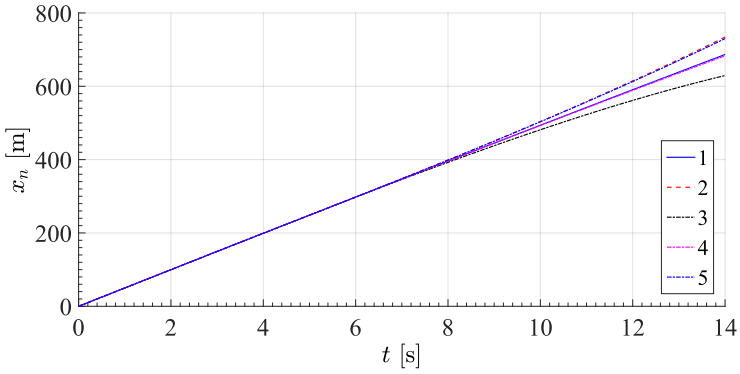

Fig. 15. Bomb range as a function of time

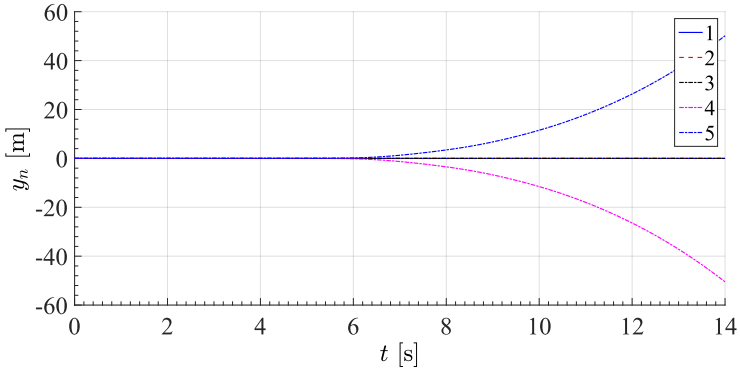

Fig. 16. Lateral bomb translation

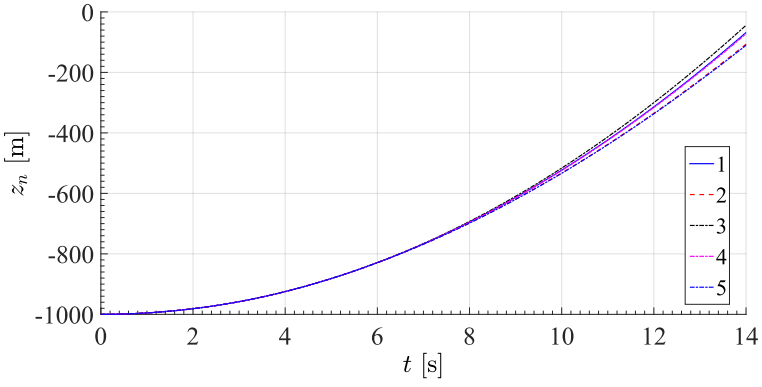

Fig. 17. Minus height of the bomb

The deviations of control flight trajectories from the uncontrolled one are very small but still observable. It shows that control loads were modeled in a proper way.

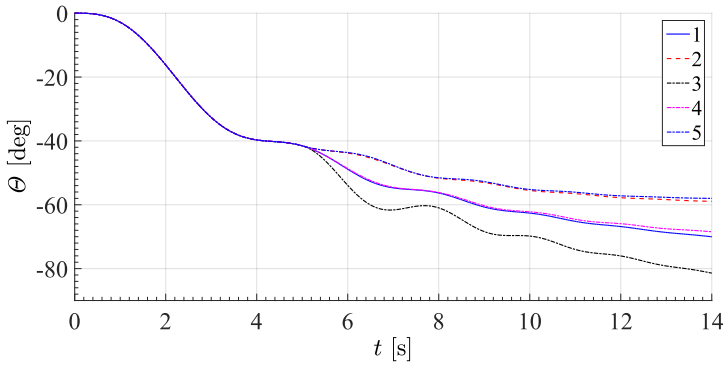

Fig. 18. Pitch angle plot

Until the fifth second, the pitch angle curves are identical for all the cases. After the fin deflection, rapid pitch oscillations are observed. In the third case, the pitch angle decreases very fast.

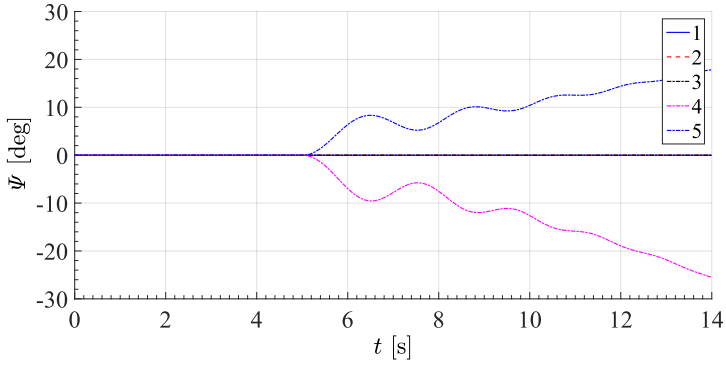

Fig. 19. Yaw angle of the bomb

The control affects clearly the bomb trajectory. The control loads model was assumed to be linear due to control derivatives. When this type of assumption is introduced, some interesting effects, like the induced roll, might be omitted. This linear type of analysis is sufficient at the early stages of design. Further simulations should be performed, especially for the maximum fin deflection angles to confirm the initial requirements. Here, only basic partial results were presented to show that the developed model works properly.

7. Conclusions

The designed bomb might be used against stationary and nonstationary targets. It can be a low-cost alternative to expensive weapons which have to be launched from big movable platforms. The proposed guidance scheme is able to ensure a

satisfactory performance during the controlled portion of trajectory. The numerical simulations indicate that the aerodynamic design was performed correctly, because the bomb was stable during the whole flight. The results of the presented work look promising. The flight dynamics model, which was developed by the Authors, can be used to derive the control laws for the bomb autopilot. Some nonlinear interference effects should be included in the overall flight dynamics model at the next design stages. Further simulation should be performed for a large set of initial velocities and heights to study the whole range of flight conditions.

Manuscript received by Editorial Board, February 27, 2018;
final version, July 04, 2018.

References

[1] J. Sabak. Defence 24. http://www.defence24.pl/106049,farnborough-ultralekkie-bomby-kierowane-dla-dronow (access: 24.10.2017) (in Polish).
[2] J. Bingham. http://www.thefifthcolumn.xyz/Forum/viewthread.php?tid=13 (access: 11.05.2017).
[3] S. Dubiel. Generalized solution for axi-symmetrical nose with minimum aerodynamic drag. *Journal of Theoretical and Applied Mechanics*, 28(3-4):513–524, 1990 (in Polish).
[4] A. Szklarski, P. Dobrzyński, B. Machowski, and J. Rosiak. Design of miniature object thrown off precision destruction, *Mechanik*, 7:676–677, 2016 (in Polish).
[5] Z. Koruba and Ł. Nocoń. Automatic control of an anti-tank guided missile based on polynomial functions. *Journal of Theoretical and Applied Mechanics*, 53(1):139–150, 2015. doi: 10.15632/jtam-pl.53.1.139.
[6] A. Martynow. *Experimental Aerodynamics*, Moscow, Obornogiz Publications, 1958.
[7] R. Głębocki. Guidance impulse algorithms for air bomb control, *Bulletin of the Polish Academy of Sciences Technical Sciences*, 60(4):825–833, 2012. doi: 10.2478/v10175-012-0096-4.
[8] E.L. Fleeman. *Missile Design System and Engineering*. American Institute of Aeronautics and Astronautics, 2012.
[9] Babcock and M. Kannapel. Numerical simulation of the free-stream characteristics of the GBU-39/B small diameter bomb. In: *2008 U.S. Air Force T&E Days Conference*, Los Angeles, CA, 5–7 February, 2008. doi: 10.2514/6.2008-1663.
[10] H.R. Sonawane and S.P. Mahulikar. Effect of missile turn rate on aircraft susceptibility to infrared-guided missile. *Journal of Aircraft*, 50(2):663–667, 2013. doi: 10.2514/1.C031902.
[11] S. Lyu, Z.H. Zhu, S. Tng, and X. Yan. Hybrid cooperative guidance law for active aircraft defense against guided missile. *Journal of Guidance, Control, and Dynamics*, 41(2):535–541, 2018. doi: 10.2514/1.G003059.
[12] M. Żugaj. UAV control system reconfiguration under physical constraints. In: *Advances in Aerospace Guidance, Navigation and Control* – Selected Papers of the 4th Specialist Conference on Guidance, Navigation and Control, pages 241–256, Warsaw, April 2017. doi: 10.1007/978-3-319-65283-2.